Materials Advances

ROYAL SOCIETY OF CHEMISTRY

PAPER

View Article Online
View Journal | View Issue

Cite this: *Mater. Adv.*, 2025, **6**, 5074

Synthesis and characterization of lignin-modified geopolymer composites for aqueous phase sequestration of methyl orange dye in a fixed-bed column

Idriss Kamdem Taquieteu,[a] Hermann Dzoujo Tamaguelon, *[a] Victor Shikuku,[b] Sylvain Tome,[a] Donald Kamdem Njouond,[c] Manelle Fouetfack Dongmo,[a] Hanibal Othman,[d] Annette Vollrath,[d] Abdulrahman Mohabbat,[d] Christoph Janiak,[d] Charles Banenzoué[a] and David Joh Daniel Dina*[a]

The present work evaluated the performance of pozzolan and sawdust derived geopolymer–lignin composites in the sequestration of methyl orange (MO) in a fixed bed as an auspicious strategy for valorization of waste sawdust. GP0, GP-CL5 and GP-CL10 composites were prepared *via* alkalination, replacing pozzolan with 0, 5 and 10% lignin (CL) extracted from sawdust, respectively. The composites were characterized using standard methods, namely X-ray diffraction (XRD), Fourier transform infrared (FTIR) spectroscopy, thermogravimetric analysis (TGA), Brunauer–Emmett–Teller (BET) surface analysis and scanning electron microscopy (SEM). The specific surface areas were decreased by the addition and increase in CL fraction from 53.4 to 24.9 $m^2\ g^{-1}$ for GP0 and GP-CL10, respectively. Incorporation of CL resulted into a poly(ferro-lignino-sialate) single-network. Addition of CL increased the breakthrough time and the operating time of the column. The Thomas model best described the breakthrough curves. MO sequestration performance (Q_0) was three times better on GP-CL10 than GP0 when the feed rate was increased. The MO fixation mechanism mainly includes external and internal diffusion and electrostatic interactions. The adsorption is driven by the surface chemistry rather than textural characteristics of the adsorbent. These results indicate that geopolymer–lignin composites are potential eco-adsorbents for the removal of azo dyes in a continuous adsorption system and presents a plausible way for recycling sawdust.

Received 19th March 2025,
Accepted 7th June 2025

DOI: 10.1039/d5ma00248f

rsc.li/materials-advances

1. Introduction

The design of sustainable, low-cost and environmentally friendly materials is increasingly recommended, especially in remote and low-income economies.[1,2] Geopolymers are new classes of amorphous or semi-crystalline aluminosilicate materials derived from the polymerization/polycondensation between an aluminosilicate source and an activating agent (an alkaline or phosphoric acid solution) at room temperature or moderately high temperature (below 100 °C).[3] Industrial wastes (blast furnace slag fly ash, dolochar, diatomaceous earth, *etc.*) and natural wastes (metakaolin, pumice, laterites and pozzolans *etc.*) are the types of precursors rich in silica- and alumina-rich precursors are widely used.[4–6] Although geopolymers are mainly used in civil engineering because of their high mechanical properties, low shrinkage, relatively low emission of carbon dioxide (CO_2) during their synthesis and their high resistance to acids, they have also proved highly efficient in encapsulation of certain toxic wastes and in the treatment of industrial effluents.[7,8] Geopolymerization products possess excellent properties (specific surface area, porosity structures and high surface functional groups) for application as geoadsorbents in the sequestration of water contaminants relative to pristine precursors.[7,9,10] However, the adsorption performance varies with the type of precursor, composition of activator, type and amount of additive or forming agent and synthesis conditions.[7,11–14] With a view to improving the intrinsic and extrinsic characteristics of these adsorbents, recent research studies have incorporated carbonaceous additives such as rice

[a] *Department of Chemistry, Faculty of Sciences, University of Douala, P.O. Box 24157, Douala, Cameroon. E-mail: hermann.dzoujo@gmail.com, dinadavidcr@yahoo.com*
[b] *Department of Physical Sciences, Kaimosi Friends University, P.O. Box 385-50309, Kaimosi, Kenya*
[c] *Department of Process Engineering, Saint Jerome Catholic University Institute, Av. Akwa Koumassi, Douala, Cameroon*
[d] *Institut für Anorganische Chemie und Strukturchemie, Universität Düsseldorf, Universitätsstr. 1D-, 40225, Düsseldorf, Germany. Tel: +49-211-81-12286*

husk ash,[15] biochar bagasse[16] and waste charcoal powder[17,18] in the geopolymer matrix resulting in densified functional groups, increased specific surface areas (SSAs) and concomitant increase in adsorption capacities. Other studies have also reported that some additives lead to diminished SSAs and composites with indistinguishable adsorption capacities.[7] However, the composites exhibited decreased tortuosity leading to increased adsorption rates. While both adsorption capacity and adsorption rate are important criteria for selecting the best performing adsorbents, the difficulty lies in the search for low-cost functional additives that exhibit increased adsorption capacity and faster kinetics, especially from waste materials. Although these incorporated additives are mostly lignocellulosic in nature, the effect of lignin alone on the physicochemical characteristics of the resulting product has not been reported in the literature, compared with cellulose, which enhances the mechanical properties.[19] Lignin (CL) is one of the carbonaceous materials derived from the by-products of pulp, paper and biomass (pre)-treatment processes.[20] Its aromatic structure and diverse functional groups give it excellent adsorptive properties in the sequestration of organic and inorganic contaminants.[21–23] Lignin extraction from sawdust using the Organosolv process is considered as a low-cost and more environmentally friendly process than the lignosulphonate, Kraft and soda lignin processes while maintaining the integrity of the extracted lignin.[24,25] Modification of metal organic framework (MOF) adsorbents using lignin additives has been reported to increase the number of active sites resulting in increased adsorption of methyl orange (MO) dye.[26,27] This could present a suitable strategy to counteract the effect of the negatively charged geopolymer framework that may limit the uptake efficiency for anionic methyl orange molecules. The synergistic or antagonistic effect of lignin-modified geopolymers is unknown given the diverse properties of geopolymers including concentrations and strength of Brønsted (BAS) and Lewis (LAS) acid sites, porosity, exchangeable cations and surface areas, all of which affect adsorption performance.[28] Methyl orange was chosen as the model adsorbate for this study because of its widespread use, persistence in the environment, high solubility, toxicity and known carcinogenicity, making its removal from wastewater critical. Its elimination by adsorption through a column packed with adsorbents compared with other traditional methods (coagulation–flocculation, membrane filtration, ozonation *etc.*) has proved to be a very efficient process due to its low operating costs, flexibility and simplicity of design.[29,30] The novelty of this study is the functionalization of geopolymers using lignin derived from sawdust waste as a new class of geopolymer composites. The use of lignin from otherwise waste material is consistent with principles of circular economy, whereas the interplay between lignin and aluminosilicates provides new insights into controlling the properties of geopolymer composites for maximization of their adsorptive properties. The aim of this study is to evaluate the structural, functional and textural activity of lignin addition on adsorptive characteristics of pozzolan-based geopolymers in the abatement of a toxic and carcinogenic methyl orange (MO) dye in a fixed-bed system under various conditions and the results are reported herein.

2. Material and methods

2.1. Precursor collection and composite synthesis

The pozzolan used came from the locality of Quanté (near Penja) in the Loum arrondissement, Moungo department, Littoral region of Cameroon with geographical coordinates 32 N 075737, UTM 0517064 at an altitude of 367 m. The collected pozzolan was washed, dried, crushed and then sieved through a 100 μm sieve. The Bunbiga sawdust waste used for lignin extraction, on the other hand, was obtained from a furniture processing and production unit in Douala-Logbessou. Lignin was extracted from 10 and 25 g of Bubinga (*Guibourtia Tessmannii*) sawdust using the organosolv process from which the mixture and 99% ethanol sawdust was thermally stirred at 180 °C for 90 min (Fig. 1). After extraction, the lignin (L) was thermally activated at 240 °C for 1 h in an electric oven at a heating rate of 10 °C min^{-1}.

The geopolymer–lignin composites were synthesized by initially substituting the pozzolan with 0, 5 and 10% calcined

Fig. 1 Schematic of lignin extraction.

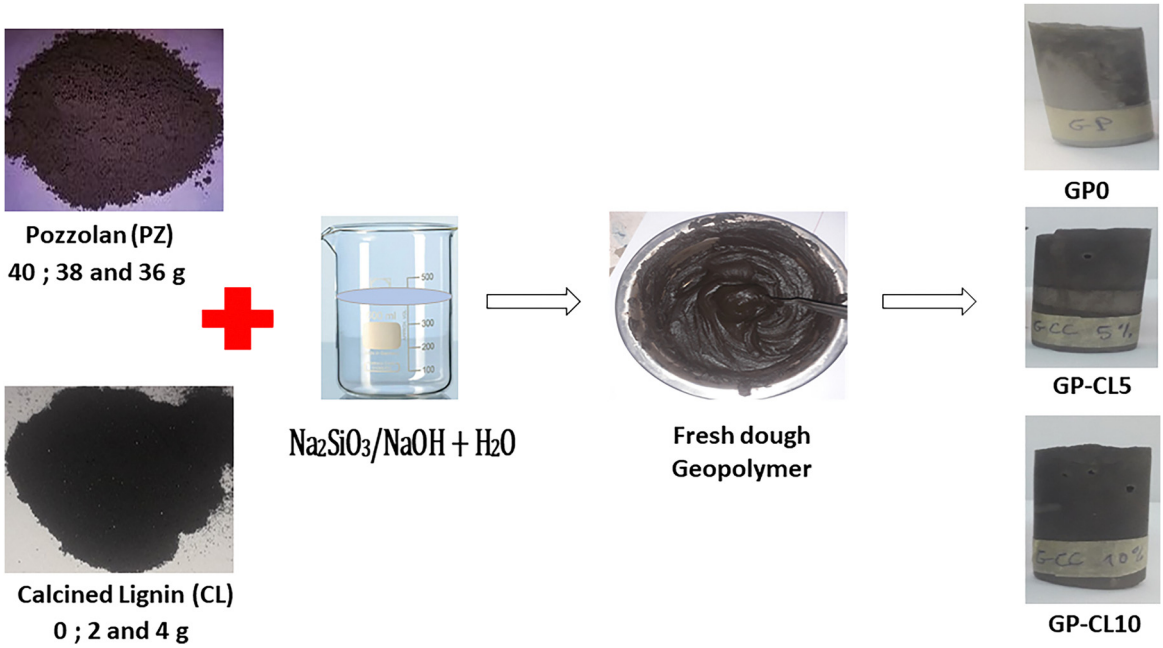

Fig. 2 Synthesis procedure of GP0, GP-CL5 and GP-CL10 geomaterials.

lignin (CL) fractions. The powders obtained were mixed with an alkaline solution (mixture of 10 mL of soda (12 M) + 24 mL of sodium silicate). The liquid/solid solution ratio used was 0.3. The different pastes were introduced into PVC moulds and oven-dried at 50 °C for 7 days to promote the geopolymerization process and also reduce the risk of degradation of lignin in the geo-composites.[31] The resulting materials denoted as GP0, GP-CL5 and GP-CL10 according to the CL proportions (Fig. 2) were ground, sieved at 100 μm, and washed with distilled water to remove excess activating agents before being oven-dried at 50 °C and packaged for characterization and adsorption testing.

2.2. Sample characterization

The different minerals contained in the precursors and composites were determined using a Discovery X-ray Bruker D8 diffractometer. The diffractograms were recorded between 6° and 80° with a step size of 0.021 at a scanning speed of 1 s per step. The main chemical functions present on the surface of the samples were identified using Fourier transform infrared spectroscopy using the KBr method on an infrared spectrometer (Perkin 156 Elmer, Shelton, CT, USA) and the spectra were recorded between 4000 and 400 cm^{-1} with a resolution of 2 cm^{-1} and 32 scans. The thermal behavior of the geomaterials was evaluated using a TA NETZSCH TG209F3 thermocouple (TA NETZSCH, New Castle, USA) between 30 and 800 °C under a nitrogen atmosphere (20 mL min^{-1}) with a heating and cooling rate of 6 K min^{-1}. The specific surface areas of the materials were evaluated by means of N_2 adsorption at 77 K using Quantachrome Autosorb AS6AG Station 3 equipment (Quantachrome, Odelzhausen, Germany) using the BET method. Morphological analysis of the samples was carried out using a scanning electron microscope (SEM, Hitachi Ltd, Japan) to visualize their internal microstructure.

2.3. Methyl orange sequestration test

Dual adsorption tests of MO in a fixed bed were performed using the device illustrated in Fig. 3. During the process, the MO effluents were injected *via* a pump (type BT100-1F Hebei, China) into the columns (with an internal diameter of 9 mm and a height of 5 to 10 mm) filled with 0.2 and 0.6 g of geomaterials. The various filtrates collected were analyzed using a UV-visible spectrophotometer at a wavelength of 465 nm to determine the residual MO concentration. Composite adsorption capacity at exhaustion (Q_e), removal rate at

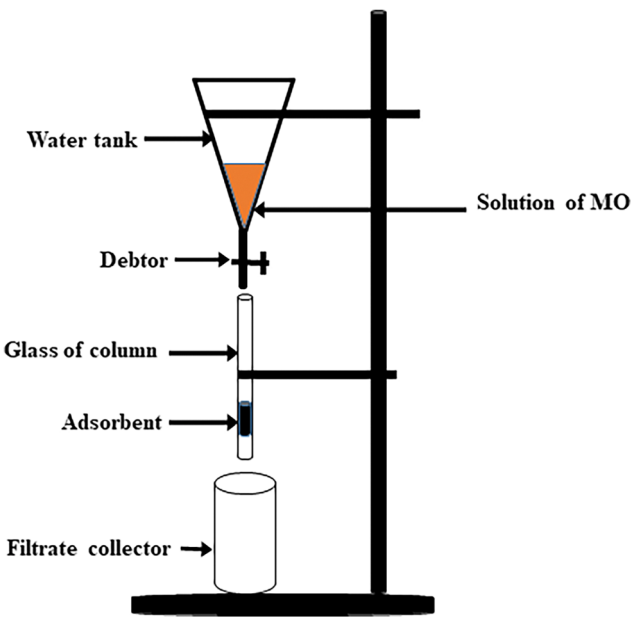

Fig. 3 Simplified column adsorption system.

breakthrough ($\%R_{t_b}$) and mass transfer zone (MTZ) were calculated using eqn (1)–(4) respectively:

$$Q_e = \frac{F}{1000m}\int_{t=0}^{t=t_e} C_{ads}\,dt = \frac{(C_0 - C_t) \times V_{eff}}{m} \quad (1)$$

with

$$C_{ads} = C_0 - C_t \text{ and } V_{eff} = F \times t_{max} \quad (2)$$

$$\%R_{t_b} = \frac{(C_0 - C_{t_b}) \times 100}{C_0} \quad (3)$$

$$MTZ = Z \times \frac{(t_e - t_b)}{t_e} \quad (4)$$

where F (mL min^{-1}) and t_e (min) represent the column feed rate and exhaustion time respectively. Q_e and $\%R_{t_b}$ are, respectively, the adsorption capacity (mg g^{-1}) and the removal rate at breakthrough time ($\%R_{t_b}$). C_0 and C_t (mg L^{-1}) are, respectively, the initial concentration and the concentration at time t_e of the MO. V_{eff} (L) and m (g) are, respectively, the volume of effluent and the dose of adsorbent in the bed. MTZ (cm), Z (cm) and t_b (min) are the mass transfer zone, bed height and breakthrough time, respectively.

2.3.1 Effect of pH. Various solutions of MO (10 mg L^{-1}) with pH values adjusted between 2 and 10 from a solution of HCl (0.1 M) or NaOH (0.1 M) were injected with a feed rate of 0.5 mL min^{-1} into different columns packed with 0.4 g of geomaterials and the residual concentrations of the effluents collected after 30 minutes were determined.

2.3.2 Effect of initial concentration. In two 9 mm diameter columns, each containing 0.6 g of geomaterials, two solutions of MO with respective concentrations of 5 and 10 mg L^{-1} were introduced at a feed rate of 0.5 mL min^{-1}, and the resulting filtrates at defined intervals were assayed using a spectrophotometer to determine the residual concentration.

2.3.3 Effect of flow rate. Using a pump fitted with a flow meter, MO solutions with a concentration of 10 mg L^{-1} were injected into 9 mm columns containing 0.6 g of material by varying the feed rates to 0.5 and 1.5 mL min^{-1} and the residual concentrations of the filtrates collected were determined.

2.3.4 Effect of bed height. In two 9 mm diameter columns packed respectively with 0.2 and 0.6 g of adsorbents, the MO solutions (10 mg L^{-1}) were injected at a feed rate of 0.5 mL min^{-1} and the residual MO concentrations of the filtrates were determined.

3. Results and discussion

3.1. Mineralogical composition

Fig. 4 shows the diffractograms of the PZ and CL precursors. The CL diffractogram shows a dome extending between 10 and 35° (2θ), confirming the amorphous nature of the extracted lignin, which is consistent with the mineralogical profile of lignin.[32] For pozzolan, a crystalline mineralogical structure is observed with certain identifiable peaks such as albite (COD_98-009-0142), anorthite (COD_98-010-0233), cristobalite (COD_98-007-7454), augite (COD_98-005-6926), biotite (COD_98-080-1110) and magnetite (COD_98-018-3972). Fig. 5 shows the diffractograms of the GP0 geopolymer and the GP-CL5 and GP-CL10 composites. GP0, GP-CL5 and GP-CL10 exhibited the majority of the minerals present in PZ. However, it is worth noting the absence of crystalline phases such as albite at 58.4° (2θ) and augite at 35.5° (2θ) within GP0, GP-CL5 and GP-CL10, reflecting their dissolution in the activating solution during the geosynthetic process. In addition, by comparing the diffractograms of GP0 with those of GP-CL5 and GP-CL10, the dome located between 10 and 35° (2θ) within the composites is more pronounced, revealing that the addition of lignin to the geopolymeric matrix favored amorphization of the network and

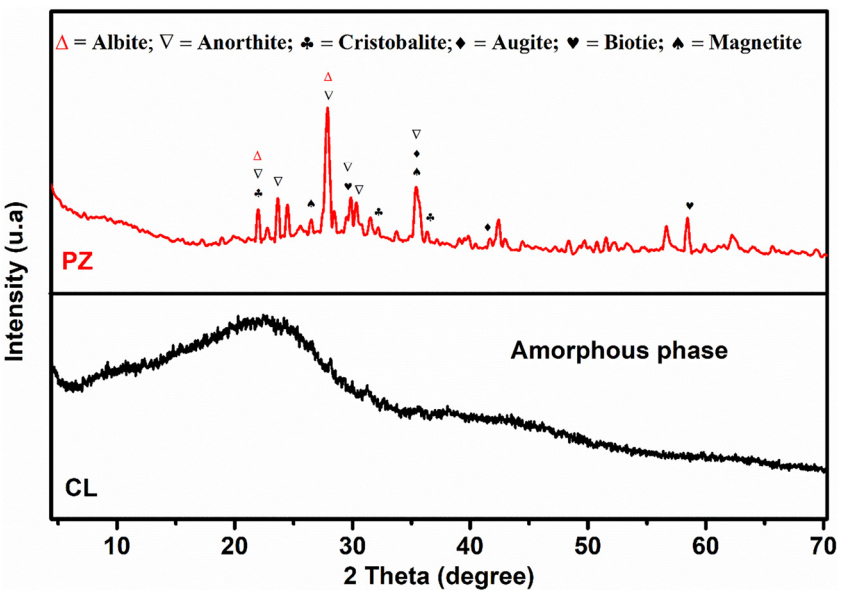

Fig. 4 XRD patterns of PZ and CL.

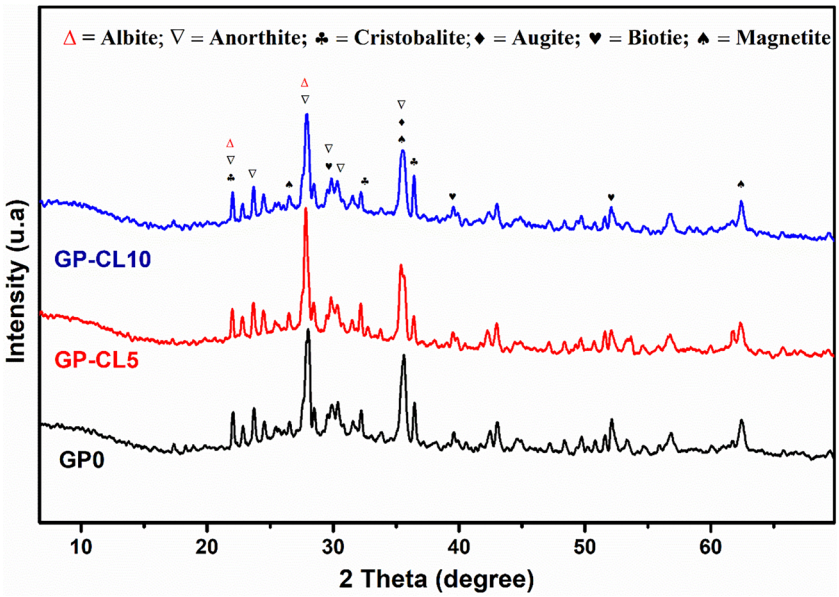

Fig. 5 XRD patterns of GP0, GP-CL5 and GP-CL10.

geopolymerization.[18] However, this geopolymerization process could be delayed when the lignin content is higher than 5% due to the reduction in the contact surface between the activating solution and the aluminosilicate source.

3.2. Functional group analysis

Fig. 6a shows the spectra of Pz and CL. In these spectra, the strong signals appearing at 3406 and 2933 cm^{-1} correspond to stretching of the hydroxyl bond (O–H) and C–H stretching vibrations of the methyl group ($–CH_3$), respectively. Bands of vibrations appearing at 1606 and 1510 cm^{-1} were attributed to aromatic framework rings of phenolic hydroxyl groups.[33] The signal at 1457 cm^{-1} corresponds to asymmetric C–H deformation with aromatic ring vibration.[33] The peak at 1269 cm^{-1} corresponds to the deformation vibrations of the guaiacyl groups. The bands at 1120 cm^{-1} can be referred to the in-plane C–H deformation bands of syringyl and guaiacyl units and the one at 1030 cm^{-1} to the C–O deformation of primary alcohols. In the PZ spectrum, the broad band observed at 3443 cm^{-1} and the weak peak at 1644 cm^{-1} are characteristic of the vibration of –OH bonds in water. The intense peak observed in the 1027 cm^{-1} region is attributed to Si–O–Si or Si–O–Al bonds. Finally, the weak peak located around 540–464 cm^{-1} is linked to the symmetrical vibrations of the Al–O–Al, Si–O–Fe and Si–O–Si.[34]

Fig. 6b shows the spectra of the GP0 geopolymer and the GP-CL5 and GP-CL10 composites. The broad bands observed around 3435 cm^{-1} and weak peaks around 1640 cm^{-1} are attributable to –OH hydroxyl bonds and the stretching and bending vibrations of H–O–H bound water molecules, which may be adsorbed on the surface or trapped in the cavity of the geopolymer and composites.[35] The high-intensity peaks at 1017 cm^{-1} are characteristic of symmetrical and asymmetrical Si–O–Al or Si–O–Si stretching in the geopolymer lattice.[16] The peaks reflecting the geopolymerization process located at 580 cm^{-1} correspond to the symmetrical elongation of Al–O–Al, Si–O–Fe and Si–O–Si.[4] By comparing the spectra of the GP-CL5 and GP-CL10 composites with those of the reference GP0 geopolymer, new low-intensity absorption peaks at around 1562 cm^{-1}; 1515 cm^{-1}, 1454 cm^{-1}, 1561 cm^{-1} and 1500 cm^{-1} were observed attributable to aromatic vibrations and deformation in the C–H plane of the calcined lignin skeleton, thus reflecting an increase in the surface chemical function in the geopolymeric network. In addition, the narrowing of the vibration peak of the aluminosilicate phases observed within the composites could reflect a structural reorganization of these phases with the incorporation of CL into the matrix.[13]

3.3. Thermal analysis

Fig. 7 shows the thermograms for the calcined lignin CL, the reference geopolymer GP0 and the composite GP-CL10. Two mass loss phases can be observed for CL and GP0, unlike GP-CL10, which has three. The first phase of mass loss located respectively between 25 and 150 °C for CL of 3%, 25 and 250 °C for GP0 of 3 and 3 for GP-CL10 corresponds to the loss of mass linked to the unbound and physically adsorbed water molecules.[29] The second phase, with a mass loss between 150 and 799 °C of 59% for CL, and between 150 and 350 °C for GP-CL10, corresponds to the degradation of the lignin in these two materials. However, the decomposition of lignin in the GP-CL10 composite confirms the presence of CL lignin in the geopolymeric matrix. The third phase, which includes a mass loss of 5% between 350 and 799 °C for GP-CL10, and the second phase observed in GP0 (1%) between 250 and 799 °C reflect the dehydroxylation of the silicate minerals present in the structure.[17]

3.4. Specific surface area and microstructural analysis

Table 1 shows the specific surface areas of the precursors L, CL, PZ and the synthesized lignin-modified geomaterials GP0, GP-CL5 and GP-CL10. Thermal activation of the lignin and geopolymerization increased the specific surface area from 0 to

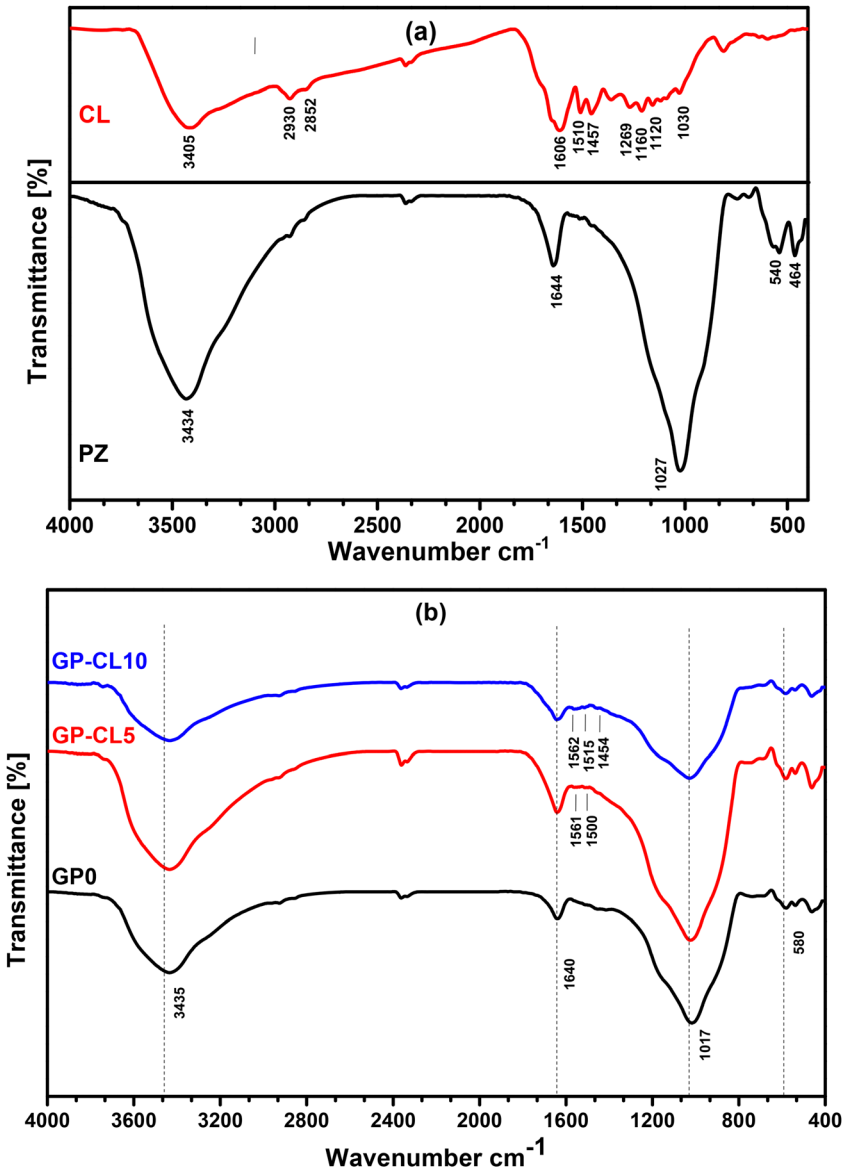

Fig. 6 FTIR spectra of precursors (a) and geomaterials (b).

2.06 $m^2 g^{-1}$ for CL/L and from 25.60 to 53.40 $m^2 g^{-1}$ for GP0/PZ, respectively. However, the addition of the CL fraction to the geopolymeric chain led to a decrease in specific surface area as a function of CL content, from 53.40 to 35.99 and 24.90 $m^2 g^{-1}$ respectively. This decrease is due to the loading of CL into the pores, which generates more bonding sites within the geopolymer network. These results are similar to those of Babazadeh *et al.*, who reported that modifying chitosan–clinoptilolite with a surfactant resulted in a reduction in the specific surface area from 21.8 to 11.5 $m^2 g^{-1}$.[29]

Fig. 8 illustrates the micrographs of the selected materials CL; GP0; GP-CL5 and GP-CL10. The microstructure of CL shows a porous and amorphous morphology, while GP0 is heterogeneous and dense due to the incomplete dissolution of the aluminosilicate phases in the alkaline solution and to the polymerization/polycondensation process. A comparison of the microstructures of the GP-CL5 and GP-CL10 composites with that of the GP0 geopolymer reveals homogeneous and increasingly less porous structures due to the occupation of the geopolymer microcavities by CL. These observations are consistent with the specific surface areas of the materials. In addition, the densification of functional groups despite porosity and specific surface area could significantly improve the adsorption performance of the resulting composites in retaining water contaminants.

3.5. Mechanism for obtaining geopolymer–lignin composites

Taking into account the mineralogical, functional and microstructural analyses, the mechanisms linked to the formation of geopolymer–lignin composites could include the dissolution of silica, alumina and iron oxides in the activating solution into silicate, aluminate and ferrate oligomers, which polymerize

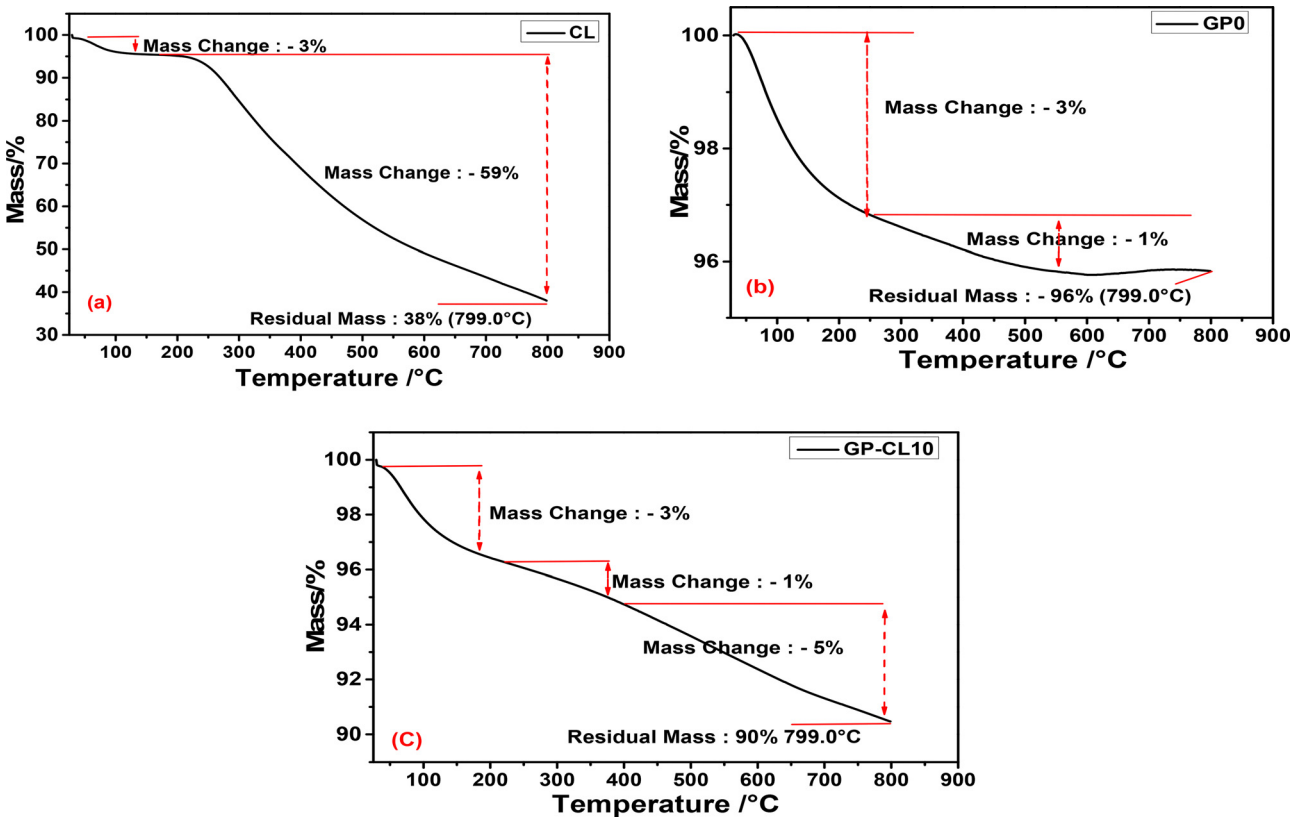

Fig. 7 Thermograms of CL (a); GP0 (b) and GP-CL10 (c).

Table 1 Specific surface area of samples

Adsorbent	Specific surface area (m^2 g^{-1})
PZ	25.60
L	0.00
LC	2.06
GP0	53.40
GP-CL5	35.99
GP-CL10	24.90

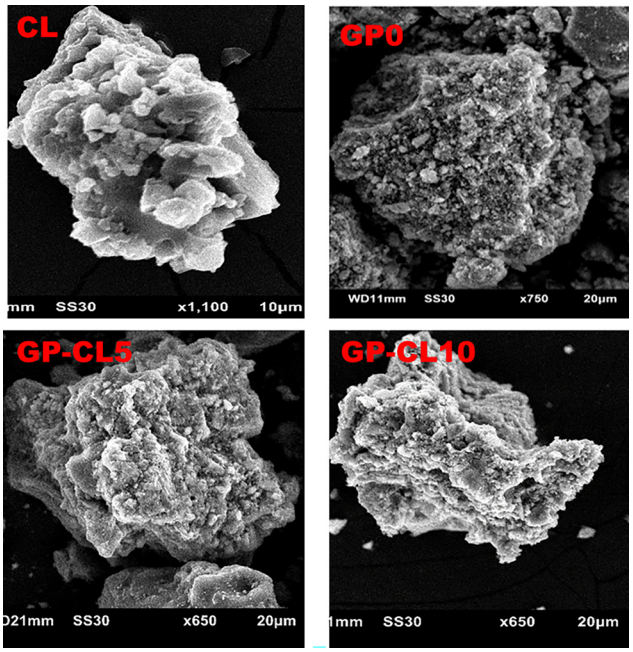

Fig. 8 Microstructures from scanning electron microscopy of CL; GP0; GP-CL5 and GP-CL10.

with the lignin. Polymerization followed by polycondensation results in the formation of a poly(ferro-lignino-sialate) chain in the network as shown in Fig. 9.

4. Adsorption study

4.1. Influence of pH

Fig. 10 shows the effect of pH on the variation in MO sequestration capacity of the GP0, GP-CL5 and GP-CL10 adsorbents. It is observed that the fixation of MO on the surface of the geomaterials is very favorable (normalized concentration <1) in a highly acidic environment (pH = 2) due to the positive surface charge of the materials generated by protonation, which induce attractive interactions with the adsorbate. At lower pH, there is also increased competition between the smaller hydrated radius of Cl^- (from HCl) and MO molecules for the same active sites. In addition, the increase in OH^- ions as the pH increases leads to deprotonation at the adsorbent surface hindering the sequestration of MO due to repulsive

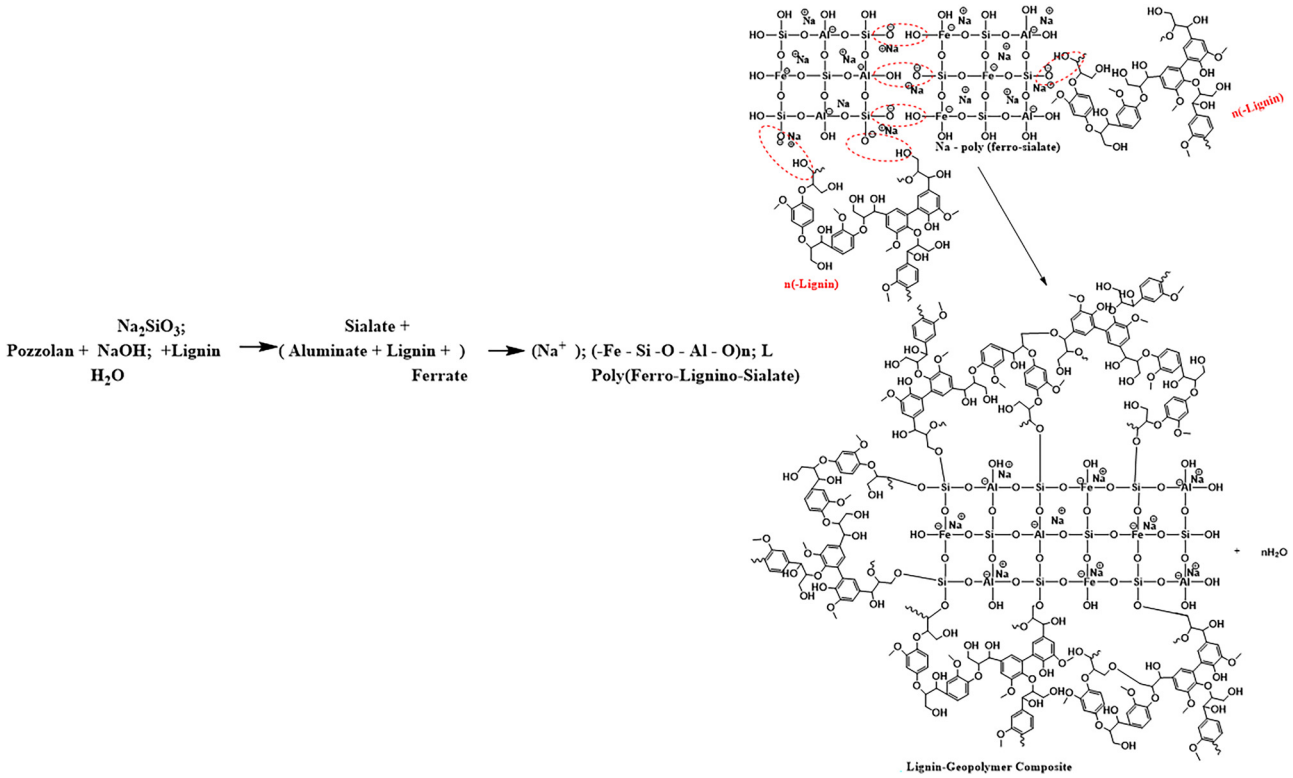

Fig. 9 Probable mechanisms linked to the consolidation of geopolymer–lignin composites.

forces with the negative surface charge of the geoadsorbents and anionic MO. At high pH, there is also competition between hydroxyl ions and the MO molecules for the same binding sites. However, FTIR analysis revealed that CL contains acid groups and their deprotonation in a basic medium could be linked to the more pronounced repulsive interactions within geopolymer composites.

4.2. Influence of initial concentration

Table 2 illustrates the parameters resulting from the effect of concentration from the breakthrough curves (Fig. 11). It is observed that the values of the breakthrough time (t_b) decrease with increasing concentration, denoting an increased distribution of the MO molecules on the surface of the materials under the impetus of the concentration gradient. However, this

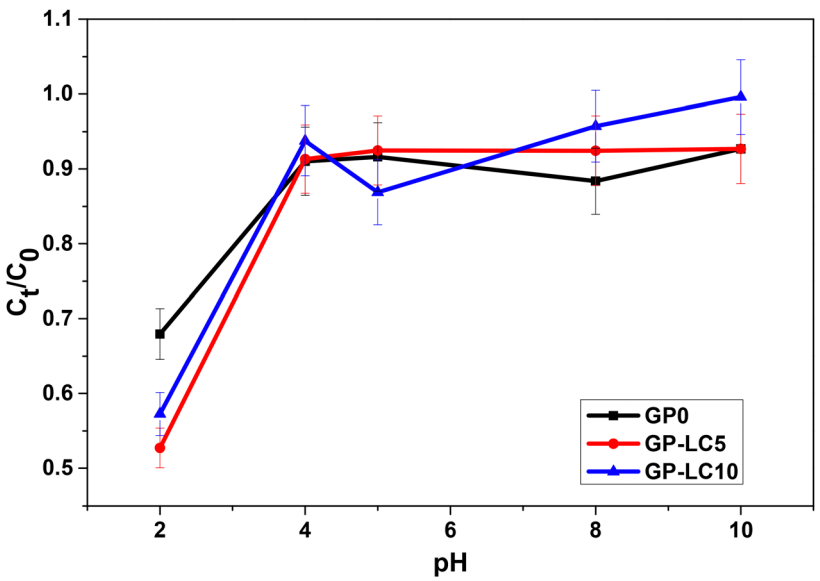

Fig. 10 Effect of pH on the adsorption of MO by GP0, GP-CL5 and GP-CL10 materials (m = 0.4 g, C_0 = 10 mg L^{-1}).

distribution time is greater inside the composites due to the contribution of the active sites provided by the CL in the geopolymeric matrix. The R_{t_b} values, which increase from 52 to 62% for GP-CL5 and from 69 to 83% for GP-CL10, confirm this hypothesis. Furthermore, the decrease in geoadsorbent adsorption capacity with the increase in MO concentration indicates saturation of the binding sites by a drastic increase in the number of adsorbate molecules.[36] In addition, the saturation time (t_e) values, which decrease with increasing concentration, indicate that the concentration flow generates strong repulsive interactions between the adsorbed MO molecules and those in the bulk solution, and consequently leads to a reduction in adsorption capacity and column operating time. These results corroborate the work of Taquieteu *et al.*[37] on MO adsorption on regenerated activated carbons.

4.3. Influence of column flow rate

The breakthrough curves and flow rate effect parameters highlighted in Fig. 12 and Table 3 respectively reveal that increasing the flow rate from 0.5 to 1.5 mL min^{-1} leads to a consistent decrease in the percentage removal from 47 to 22% for GP0, from 52 to 39% for GP-CL5 and from 69 to 58% for GP-CL10 due to the short contact time between the adsorbent and the adsorbate. However, when the flow rate is increased from 0.5 to 1.5 mL min^{-1}, a significant increase in the adsorption capacity (Table 3) of the bed with the composites is observed. This reflects an increase in surface diffusion phenomena in the bed column favored by the increase in binding sites. It was also found that saturation times characterized by a reduction in MTZ become relatively shorter as the flow rate increases, due to the mass gradient of the MO, which accelerates saturation of the active sites. Similar results were obtained for the adsorption of methylene blue dye and permanganate ion by pyrolytic tyre charcoal and a chitosan–*Ocimum basilicum* leaf–ZnO composite membrane respectively.[38,39]

4.4. Influence of bed height

Table 4 highlights the parameters derived from the breakthrough curves (Fig. 13) of the influence of the bed height. It is observed that increasing the bed height leads to a more significant increase in the breakthrough time of the composites compared to GP0 due to the contribution of the binding sites provided by CL in the geopolymer matrix to improve the mass transfer zone.[40,41] As a result, an increase in the removal rate is recorded. Furthermore, the saturation times (t_e) of the geocomposites, which increased with the height of the bed in contrast to the MO adsorption capacities, indicate that the sequestration of MO does not depend solely on the number of active sites per gram of adsorbent but also on the textural properties. Consequently, this decrease in adsorption capacity is linked to the reduction in specific surface area with the addition of CL to the geopolymer matrix. These results are not consistent with the literature, which reports that increasing MTZ with increasing height provides more binding sites for adsorbate sequestration.[29,36]

It was found that the initial MO concentration and the flow rate are the parameters most likely to influence the saturation time of columns packed with geopolymer composites. The resulting experimental data were used in mathematical models to predict the model that best fits the influence of these parameters.

Table 2 Parameters relating to the influence of the initial concentration of MO

C_0 (mg L^{-1})	Adsorbent	t_b (min)	t_e (min)	MTZ (cm)	Q_e (mg g^{-1})	$\%R_{t_b}$
5	GP0	30	160	0.81	0.211	47
	GP-CL5	50	180	0.72	0.292	52
	GP-CL10	100	200	0.50	0.353	69
10	GP0	10	150	0.93	0.210	25
	GP-CL5	50	150	0.67	0.271	62
	GP-CL10	80	170	0.53	0.313	83

4.5. Breakthrough curve models

The Thomas,[42] Bohart–Adams[43] and Yoon–Nelson[44] models, expressed by eqn (5)–(7) respectively, were used to predict the behaviour of the fixed-bed column and estimate the parameters required for the design. The adequacy of these empirical models to correlate with the experimental data was examined *via* the coefficient of determination (R^2) associated with the mean relative error function (eqn (8)).

$$\left(\frac{C_t}{C_0}\right) = \frac{1}{1 + \exp\left(\frac{K_{TH} Q_0 m}{F} - C_0 K_{TH} t\right)} \quad (5)$$

$$\left(\frac{C_t}{C_0}\right) = \exp\left(K_{AB} C_0 t - \frac{K_{AB} N_0 Z}{\nu}\right) \quad (6)$$

$$\left(\frac{C_t}{C_0}\right) = \exp(K_{YN} t - K_{YN}\tau) \quad (7)$$

$$ARE = \frac{100}{n}\sum_{1}^{n}\left|\frac{\left(\frac{C_t}{C_0}\right)_{EXP} - \left(\frac{C_t}{C_0}\right)_{CaL}}{\left(\frac{C_t}{C_0}\right)_{EXP}}\right| \quad (8)$$

where: K_{TH}: is the Thomas constant; Q_0: is the maximum adsorption capacity of the solute on the adsorbent (mg g^{-1}); t: is the breakthrough time (min); v: is the velocity in the reactor assumed to be empty (cm min^{-1}); N_0: is the dynamic adsorption capacity; Z: is the packing height (cm); K_{AB}: is the Bohart–Adams constant; K_{YN}: is the Yoon–Nelson constant; τ: is the time corresponding to adsorption of 50% adsorbate (min).

From Table 5, the Thomas model was adequate to define the removal kinetics of MO on geoadsorbents due to the relatively high $R^2 > 0.90$ and low ARE error function values. This model indicates that external and internal diffusion of MO is not the kinetically limiting step. In addition, the values of Q_0 and K_{TH}, which increase significantly with the flow rate (F) in contrast to the adsorbate concentration (C_0) at the surface of the geocomposite compared to GP0 attest that the diffusion and sequestration of MO through the column is not controlled by the textural properties but rather by the number of binding sites found at the

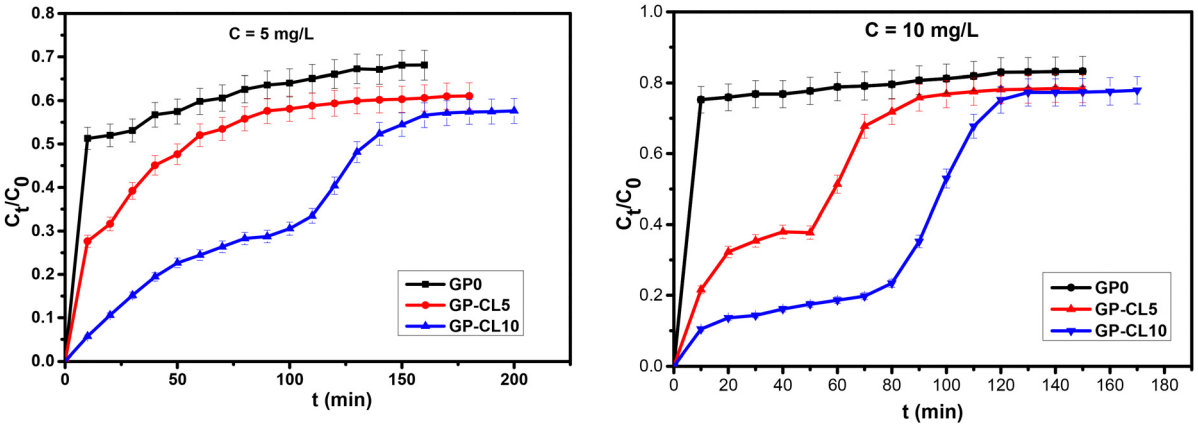

Fig. 11 Breakthrough curves for MO adsorption at different concentrations (F = 0.5 mL min^{-1}; D = 9 mm; m = 0.6 g and pH = 2).

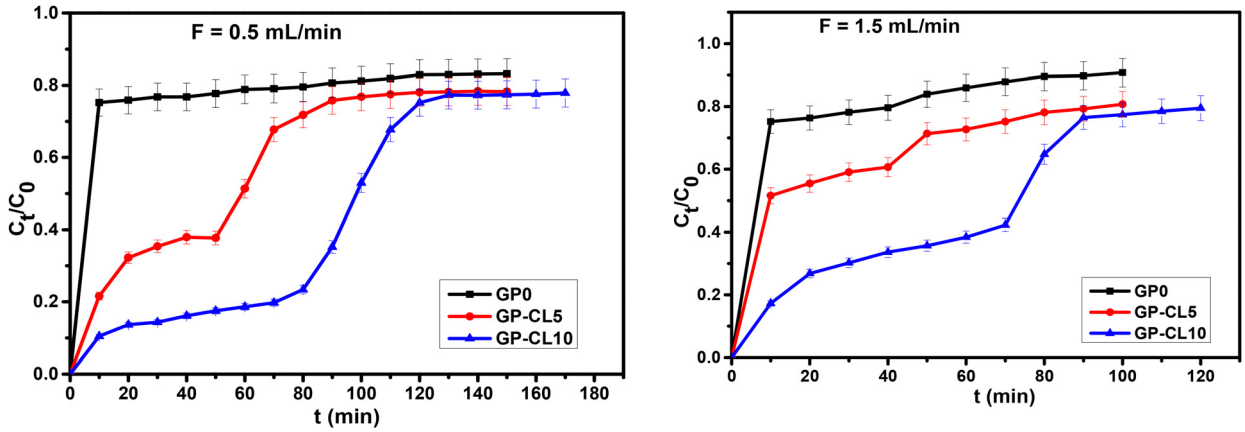

Fig. 12 Breakthrough curves for MO adsorption at different flow rates (C = 10 mg L^{-1}; D = 9 mm; m = 0.6 g and pH = 2).

Table 3 Parameters obtained for influencing flow rate

F (mL min^{-1})	Adsorbent	t_b (min)	t_e (min)	MTZ (cm)	Q_e (mg g^{-1})	$\%R_{t_b}$
0.5	GP0	10	150	0.93	0.210	47
	GP-CL5	50	150	0.67	0.271	52
	GP-CL10	80	170	0.53	0.313	69
1.5	GP0	10	100	0.90	0.231	22
	GP-CL5	40	100	0.60	0.481	39
	GP-CL10	70	120	0.42	0.615	58

Table 4 Parameters obtained for the influence of the height of the adsorption bed

Z (mm)	Adsorbent	t_b (min)	t_e (min)	MTZ (cm)	Q_e (mg g^{-1})	$\%R_{t_b}$
2.5	GP0	10	70	0.85	0.071	18
	GP-CL5	40	80	0.13	0.265	31
	GP-CL10	50	80	0.38	0.384	32
10	GP0	10	150	0.93	0.210	47
	GP-CL5	50	150	0.67	0.271	52
	GP-CL10	80	170	0.53	0.313	69

surface of these composites. The evolution of these parameters contradicts the literature, which generally indicates that the decrease in q_0 and K_{TH} with increasing flow rate is linked to the decrease in residence time, advocating saturation of the active sites.[45] Furthermore, the values of τ derived from the Yoon–Nelson model, which decreased with increasing adsorbate concentration and flow rate, reflect a more pronounced loss of efficiency in the column operating time of the GP0 packed column compared to the composites, corroborating the saturation times predicted by the experimental data. However, this model is unsuitable for describing breakthrough curves on geoadsorbents because of the high ARE values. In addition, the bed saturation concentration (N_0) values, which increase with C_0 and F, reflect the limitation of the composites active sites to bind all the MO molecules due to their low deficits in textural characteristics with the integration of CL into the geopolymeric chain. In addition, the K_{AB} values that increase with increasing flow rate indicate that external mass transfer in the initial part of the adsorption dominated the overall kinetics of the system.[46] However, the values of $R^2 > 0.90$ and the appreciable errors indicate that the Bohart–Adams model is also able to explain part of the breakthrough curves.

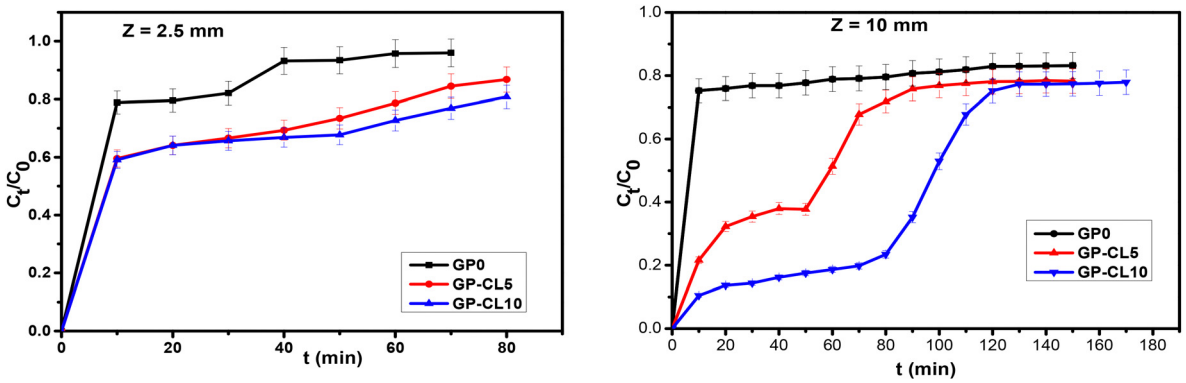

Fig. 13 Breakthrough curves for MO adsorption at different bed heights (F = 0.5 mL min^{-1}; D = 9 mm; C = 10 mg L^{-1} and pH = 2).

Table 5 Parameters calculated from kinetic models of MO adsorption in a column (D = 9 mm) packed with GP0, GP-CL5 and GP-CL10

Column conditions			Thomas model				Bohart–Adams model				Yoon–Nelson model			
F (mL min^{-1})	Z (mm)	C_0 (mg L^{-1})	K_{TH} ($\times10^{-3}$ L mg^{-1} min^{-1})	Q_0 (mg g^{-1})	ARE	R^2	K_{AB} ($\times10^{-3}$ L mg^{-1} min^{-1})	N_0 (mg L^{-1})	ARE	R^2	K_{YN} ($\times10^{-2}$ min^{-1})	τ (min)	ARE	R^2
GP0														
0.5	10	5	1.19	0.27	0.68	0.97	0.60	1149.34	0.64	0.97	0.6	63.76	1.33	0.97
0.5	10	10	6.36	0.14	3.71	0.92	0.97	782.02	3.78	0.91	0.30	31.83	11.80	0.89
1.5	10	10	1.08	0.39	2.67	0.95	0.89	2019.72	5.72	0.81	3.25	11.70	25.83	0.88
GP-CL5														
0.5	10	5	2.19	0.24	0.96	0.97	1.07	732.84	1.10	0.97	1.06	56.30	2.01	0.97
0.5	10	10	7.37	0.22	3.56	0.96	1.58	774.07	4.40	0.95	3.64	53.34	8.10	0.95
1.5	10	10	6.72	0.46	2.86	0.94	0.98	2346.59	4.72	0.87	2.60	29.04	12.77	0.92
GP-CL10														
0.5	10	5	6.77	0.35	6.00	0.96	4.48	440.57	5.26	0.96	3.45	82.74	8.84	0.96
0.5	10	10	1.06	0.31	12.8	0.94	3.21	760.99	11.06	0.92	4.63	75.58	18.92	0.91
1.5	10	10	5.90	0.95	6.29	0.93	1.77	2673.27	6.71	0.93	3.10	75.27	9.31	0.94

4.6. Mechanism of MO adsorption on the GP-CL composite

Fig. 14 illustrates the probable mechanisms of removal of MO from the geocomposite, which takes place in two phases. The first phase highlights the adsorption of MO from the ferrosialate active sites of the geopolymeric chain and the second phase, which takes place with the active sites, present on the surface of the calcined lignin of the geopolymeric network. Electrostatic interactions between the negative sites of the GP-CL composites resulting from the geopolymerization and the positive sites of the MO resulting from the acidification of the medium by the HCl located at the quaternary nitrogen level, ionic exchanges between anionic MO and the Na^+, K^+ and Ca^{2+} cations from the pozzolan and the activation solution, the π–π interactions between the aryl groups of the lignin contained in the geopolymer matrix of the geocomposites and the benzyl group of the MO, the formation of hydrogen bonds between the azo and sulphonate groups of the MO and the hydroxyl functions present in the lignin are the probable mechanisms linked to the sequestration of the MO on GP-CL. These interactions are similar to those reported by Gamal *et al.*[47] on the adsorption of methyl orange by palm and date palm spikelet-based composites.

4.7. Comparison with other adsorbents

Table 6 shows a comparison of the efficiency of the composites in this study and those in the literature with respect to anionic dyes as a function of the operating conditions. It is observed that the GP-CL10 composite has a longer exhaustive time and a higher adsorption capacity than those reported respectively in the work of Zheng *et al.*[48] and Zhao *et al.*[49] However, a lack of data on the characteristics and operating conditions of the unmodified adsorbents cannot explain the high efficiency of most of the composites in the previous work compared with those in this study.

5. Conclusion

This work reports the performance of geopolymer composites derived from pozzolan and lignin (CL) extracted from sawdust in the sequestration of the azo dye methyl orange (MO) in a fixed-bed system under various conditions. The incorporation of 10% CL into the geopolymer matrix resulted in a 53% reduction in specific surface area. However, this was compensated by the new functional groups resulting in increased

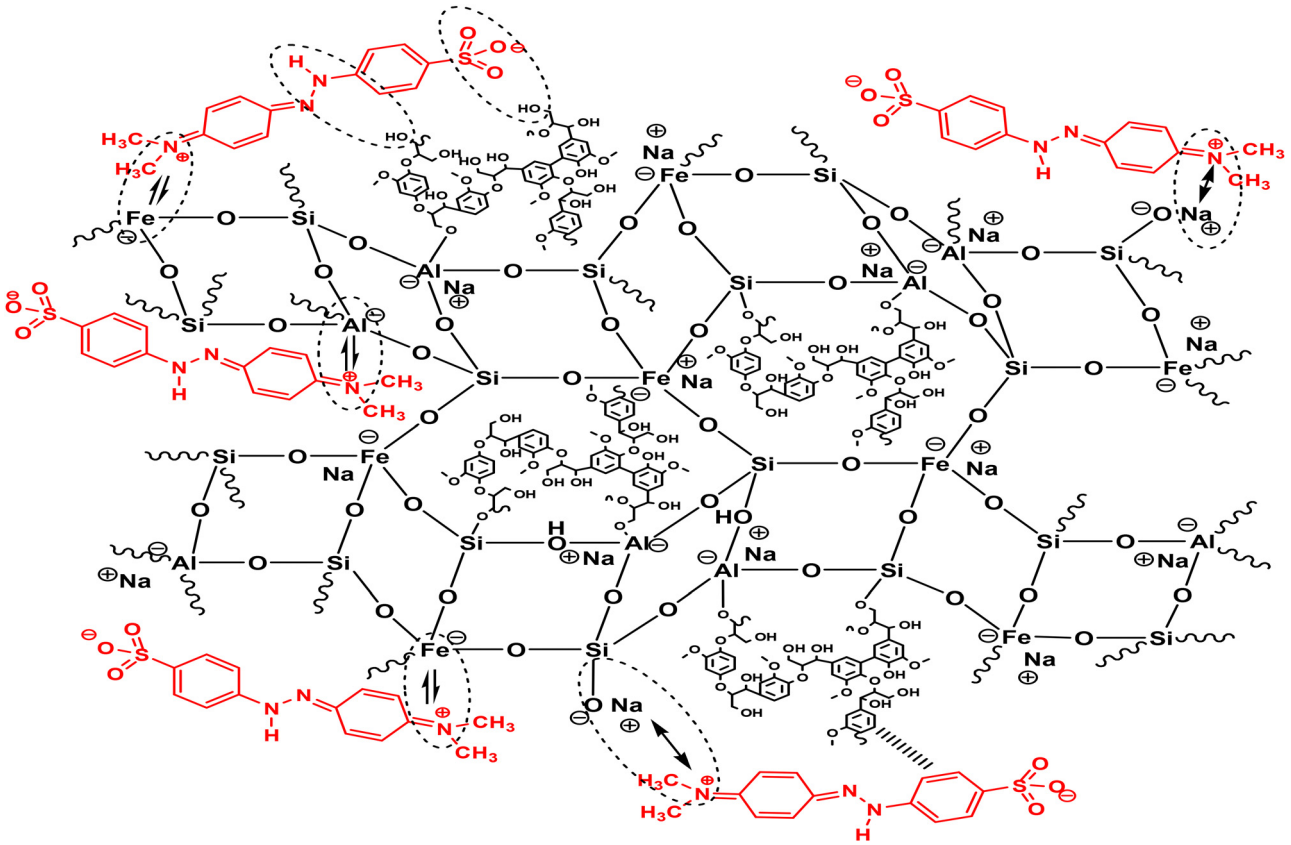

Fig. 14 Adsorption mechanism of MO on the geopolymer–lignin composite.

Table 6 Comparative adsorption performance data between the composites in this study and those from previous work with anionic dyes

			Operational conditions				Adsorption capacity	
Adsorbent	S_{BET} ($m^2\ g^{-1}$)	Anionic dyes	C_0 ($mg\ L^{-1}$)	Z (cm)	F ($mL\ min^{-1}$)	t_e (min)	Q_e ($mg\ g^{-1}$)	Ref.
PANI-ES	ND	Eosin yellow	375	2	0.3	500	67.5	50
PMC	ND	Rose bagel	400	9	3	3780	539.04	51
GCs	16.7	Direct deep blue		—	—	—	—	
TiO_2@GCs	38.4	Direct deep blue	20	1.5	5	58	106.26	48
NCL	21.8	Methyl orange		—	—	—	—	
SMCSCL composite	11.5	Methyl orange	100	1.4	7.5	ND	32.09	29
Biocomposite beads	2.74	Methyl orange	10	7.0	0.16	240	84.66	30
Iron oxide-coated zeolite	ND	Methyl orange	30	6	11	ND	0.33	49
GP0	53.40	Methyl orange	10	1.0	1.5	100	0.39	This study
GP-CL5	35.99	Methyl orange	10	1.0	1.5	100	0.46	This study
GP-CL10	24.90	Methyl orange	10	1.0	1.5	120	0.95	This study

ND: not determined.

performance. The adsorption of MO is largely controlled by the surface chemistry of the composite and not textural characteristics. Incorporation of CL also increases the saturation time (t_e) of the column by 20 min. The breakthrough curves were best described by the Thomas model. MO sequestration performance (Q_0) is 3 times better on GP-CL10 than GP0 when the feed rate is increased. The results of this study demonstrate the ability of geopolymer–lignin composites to remove azo dyes while improving column run time and open up a new challenge in the design of geopolymer composites with ultra-high adsorption densities for the removal of this class of contaminants in multicomponent systems and saline environments.

Author contributions

Idriss Kamdem Taquieteu and Hermann Dzoujo Tamaguelon: conceptualization, validation, investigation, methodology, writing – review & editing, visualization, original draft. Victor Shikuku and Sylvain Tome: validation, writing – review & editing.

Donald Kamdem Njouond, Manelle Fouetfack Dongmo, Hanibal Othman, Annette Vollrath and Abdulrahman Mohabbat: original draft, resources. Christoph Janiak, Charles Banenzoué and David Joh Daniel Dina: validation, resources, supervision. All authors read and approved the final manuscript.

Data availability

The data supporting the conclusions in this article have been included in the manuscript.

Conflicts of interest

The authors have no relevant financial or non-financial interests to disclose.

Acknowledgements

The authors declare that no funds, grants, or other forms of support were received during the preparation of this manuscript.

References

1 J. B. Njewa and V. O. Shikuku, Recent advances and issues in the application of activated carbon for water treatment in Africa: a systematic review (2007–2022), *Appl. Surf. Sci. Adv.*, 2023, **18**, 100501.
2 E. C. Ngeno, K. E. Mbuci, M. C. Necibi, V. O. Shikuku, C. Olisah and R. Ongulu, *et al.*, Sustainable re-utilization of waste materials as adsorbents for water and wastewater treatment in Africa: recent studies, research gaps, and way forward for emerging economies, *Environ. Adv.*, 2022, **9**, 100282.
3 J. Davidovits, *GEOPOLYMER CEMENTGeopolymer Cement a review, published in Geopolymer Science and Technics, Technical*, Geopolymer Institute Library, 2013, pp. 1–11, **https://www.geopolymer.org**.
4 S. Tome, A. Nana, H. K. Tchakouté, J. Temuujin and C. H. Rüscher, Mineralogical evolution of raw materials transformed to geopolymer materials: a review, *Ceram. Int.*, 2024, **50**(19), 35855–35868.
5 S. N. Fifinatasha, A. M. Mustafa Al Bakri, H. Kamarudin, Y. Zarina, A. R. Rafiza and J. Liyana, Reviews on the different sources materials to the geopolymer performance, *Adv. Environ. Biol.*, 2013, **7**(SPEC. ISSUE 12), 3835–3842.
6 J. N. Y. Djobo and S. Tome, Insights into alkali and acid-activated volcanic ash-based materials: a review, *Cem. Concr. Compos.*, 2024, **152**, 105660, DOI: **10.1016/j.cemconcomp.2024.105660**.
7 C. Onyango, W. Nyairo, B. Kwach, V. Shikuku, T. Sylvain and H. D. Tamaguelon, *et al.*, Synthesis of pumice and medical waste incinerator fly ash based phosphate geopolymers for methylene blue dye adsorption: co-valorization, parameters and mechanism, *Mater. Adv.*, 2024, **5**(21), 8546–8563.
8 E. K. Owino, V. O. Shikuku, W. N. Nyairo, C. O. Kowenje and B. Otieno, Valorization of solid waste incinerator fly ash by geopolymer production for removal of anionic bromocresol green dye from water: kinetics, isotherms and thermodynamics studies, *Sustainable Chem. Environ.*, 2023, **3**, 100026.
9 V. O. Shikuku, S. Tome, D. T. Hermann, G. A. Tompsett and M. T. Timko, Rapid Adsorption of Cationic Methylene Blue Dye onto Volcanic Ash – metakaolin Based Geopolymers, *Silicon*, 2022, **14**(15), 9349–9359, DOI: **10.1007/s12633-021-01637-9**.
10 A. S. Sidjou, A. N. Tchakounte, V. Shikuku, I. Lenou, R. Djimtibaye and M. M. Dika, Synthesis of alkali-activated volcanic scoria and rice husk ash based composite materials for adsorptive removal of crystal violet: optimization, kinetics, isotherms and mechanism, *Hybrid Adv.*, 2023, **4**, 100113.
11 S. Tome, H. Dzoujo, V. Shikuku, A. Nana, M. Annie and C. Rüscher, *et al.*, Elimination of malachite green from aqueous and saline water by laterite-derived Na-polyferrosialate and polyferrophosphosialate geopolymers: a comparative study, *Ceram. Int.*, 2023, **50**(4), 5982–5991, DOI: **10.1016/j.ceramint.2023.11.252**.
12 A. A. Siyal, M. R. Shamsuddin and A. Low, Fly ash based geopolymer for the adsorption of cationic and nonionic surfactants from aqueous solution – A feasibility study, *Mater. Lett.*, 2021, **283**, 128758.
13 H. Dzoujo, V. Odhiambo, S. Tome, F. Gallo, P. Ondiek and T. Strothmann, *et al.*, Unary adsorption of sulfonamide antibiotics onto pozzolan-tyre ash based geopolymers: isotherms, kinetics and mechanisms, *Chem. Eng. Res. Des.*, 2024, **206**, 440–452, DOI: **10.1016/j.cherd.2024.05.009**.
14 I. Luttah, D. O. Onunga, V. O. Shikuku, B. Otieno and C. O. Kowenje, Removal of endosulfan from water by municipal waste incineration fly ash-based geopolymers: adsorption kinetics, isotherms, and thermodynamics, *Front. Environ. Chem.*, 2023, **4**, 1–13.
15 S. Tome, V. Shikuku, H. Dzoujo, S. Akiri, M. Annie and C. Rüscher, *et al.*, Efficient sequestration of malachite green in aqueous solution by laterite – rice husk ash – based alkali – activated materials: parameters and mechanism, *Environ. Sci. Pollut. Res.*, 2023, 1–15, DOI: **10.1007/s11356-023-27138-3**.
16 H. Dzoujo Tamaguelon, V. O. Shikuku, S. Tome, S. Akiri, N. M. Kengne and S. Abdpour, *et al.*, Synthesis of pozzolan and sugarcane bagasse derived geopolymer-biochar composites for methylene blue sequestration from aqueous medium, *J. Environ. Manage.*, 2022, **318**, 115533, DOI: **10.1016/j.jenvman.2022.115533**.
17 J. M. Mboka, H. D. Tamaguelon, V. Shikuku, S. Tome, V. F. Deugueu and H. Othman, *et al.*, Novel Superadsorbent from Pozzolan-Charcoal based Geopolymer Composite for the Efficient Removal of Aqueous Crystal Violet, *Water, Air, Soil Pollut.*, 2024, **235**(6), 1–17, DOI: **10.1007/s11270-024-07257-4**.
18 J. M. Mboka, H. D. Tamaguelon, V. O. Shikuku, S. Tome, R. Pokeya and D. K. Njouond, *et al.*, Synergistic co-adsorptive removal of crystal violet and chromium(VI) from water by pozzolan-charcoal based geopolymer composites, *Mater. Adv.*, 2024, **5**(15), 6234–6247.
19 H. Ye, Y. Zhang, Z. Yu and J. Mu, Effects of cellulose, hemicellulose, and lignin on the morphology and

mechanical properties of metakaolin-based geopolymer, *Constr. Build. Mater.*, 2018, **173**, 10–16.

20 X. Meng, B. Scheidemantle, M. Li, Y. Y. Wang, X. Zhao and M. Toro-González, *et al.*, Synthesis, Characterization, and Utilization of a Lignin-Based Adsorbent for Effective Removal of Azo Dye from Aqueous Solution, *ACS Omega*, 2020, **5**(6), 2865–2877.

21 A. Cemin, F. Ferrarini, M. Poletto, L. R. Bonetto, J. Bortoluz and L. Lemée, *et al.*, Characterization and use of a lignin sample extracted from Eucalyptus grandis sawdust for the removal of methylene blue dye, *Int. J. Biol. Macromol.*, 2021, **170**, 375–389.

22 T. Chimi, B. U. Hannah, N. M. Lincold, M. B. Jacques, S. Tome and D. T. Hermann, *et al.*, Preparation, characterization and application of H_3PO_4-activated carbon from Pentaclethra macrophylla pods for the removal of Cr(VI) in aqueous medium, *J. Iran. Chem. Soc.*, 2023, **20**(2), 399–413.

23 R. Salih, Z. Veličković, M. Milošević, V. P. Pavlović, I. Cvijetić and I. V. Sofrenić, *et al.*, Lignin based microspheres for effective dyes removal: design, synthesis and adsorption mechanism supported with theoretical study, *J. Environ. Manage.*, 2023, **326**, 116838.

24 H. Ľudmila, J. Michal, Š. Andrea and H. Aleš, Lignin, Potential Products And Their Market Value, *Wood Res.*, 2015, **60**(6), 973–986.

25 Z. Strassberger, S. Tanase and G. Rothenberg, The pros and cons of lignin valorisation in an integrated biore fi nery, *RSC Adv.*, 2014, 25310–25318.

26 C. Wang, C. Xing, X. Feng, S. Shang, H. Liu and Z. Song, *et al.*, Lignin-modified metal–organic framework as an effective adsorbent for the removal of methyl orange, *Int. J. Biol. Macromol.*, 2023, **250**, 126092.

27 C. Wang, X. Feng, S. Shang, H. Liu, Z. Song and H. Zhang, Adsorption of methyl orange from aqueous solution with lignin-modified metal–organic frameworks: selective adsorption and high adsorption capacity, *Bioresour. Technol.*, 2023, **388**, 129781.

28 P. K. Seelam, H. Sreenivasan, S. Ojala, S. Pitkäaho, T. Laitinen and H. Niu, *et al.*, Modified geopolymers as promising catalyst supports for abatement of dichloromethane, *J. Cleaner Prod.*, 2021, **280**, 124584.

29 M. Babazadeh, H. Abolghasemi, M. Esmaeili and A. Ehsani, Comprehensive batch and continuous methyl orange removal studies using surfactant modified chitosan-clinoptilolite composite, *Sep. Purif. Technol.*, 2021, **267**, 118601.

30 S. Mirzaei and V. Javanbakht, Dye removal from aqueous solution by a novel dual cross-linked biocomposite obtained from mucilage of Plantago Psyllium and eggshell membrane, *Int. J. Biol. Macromol.*, 2019, **134**, 1187–1204.

31 P. Duan, C. Yan, W. Zhou and W. Luo, Fresh properties, mechanical strength and microstructure of fly ash geopolymer paste reinforced with sawdust, *Constr. Build. Mater.*, 2016, **111**, 600–610.

32 R. Alvarenga, C. Gomide, A. Carolina, S. De Oliveira, D. Aparecida and C. Rodrigues, Development and Characterization of Lignin Microparticles for Physical and Antioxidant Enhancement of Biodegradable Polymers, *J. Polym. Environ.*, 2020, **28**, 1326–1334.

33 D. Watkins, M. Nuruddin, M. Hosur, A. Tcherbi-Narteh and S. Jeelani, Extraction and characterization of lignin from different biomass resources, *J. Mater. Res. Technol.*, 2015, **4**(1), 26–32.

34 J. N. Y. Djobo, S. Kumar, A. Elimbi and H. K. Tchakouté, Reactivity of volcanic ash in alkaline medium, microstructural and strength characteristics of resulting geopolymers under different synthesis conditions, *J. Mater. Sci.*, 2016, **51**, 10301–10317.

35 S. Tome, M.-A. Etoh, J. Etame and K. Sanjay, Characterization and leachability behaviour of geopolymer cement synthesised from municipal solid waste incinerator fly ash and volcanic ash blends, *Recycling*, 2018, **3**(4), 50.

36 S. M. Alardhi, T. M. Albayati and J. M. Alrubaye, Adsorption of the methyl green dye pollutant from aqueous solution using mesoporous materials MCM-41 in a fixed-bed column, *Heliyon*, 2020, **6**, e03253.

37 I. K. Taquieteu, H. T. Dzoujo, V. O. Shikuku, C. Banenzou, D. David and J. Dina, Fixed-Bed Adsorption of an Azo Dye (Methyl Orange) onto Chemically and Thermally Regenerated Activated Carbons, *J. Chem.*, 2023, **2023**(1), 6677710.

38 V. Makrigianni, A. Giannakas, D. Hela, M. Papadaki and I. Konstantinou, Adsorption of methylene blue dye by pyrolytic tire char in fixed-bed column, *Desalin. Water Treat.*, 2017, **65**, 346–358.

39 M. Hemdan, A. H. Ragab, H. A. El-Siaad, J. K. Kamel, N. F. Gumaah and M. F. Mubarak, Sustainable synthesis and environmental application of chitosan-Ocimum basilicum leaves-ZnO composite membrane for permanganate ion removal in wastewater treatment, *Environ. Sci. Pollut. Res.*, 2024, **31**(58), 66164–66183, DOI: **10.1007/s11356-024-35612-9**.

40 O. Allahdin, S. C. Dehou, M. Wartel, P. Recourt, M. Trentesaux and J. Mabingui, *et al.*, Chemical Engineering Research and Design Performance of FeOOH-brick based composite for Fe(II) removal from water in fixed bed column and mechanistic, *Chem. Eng. Res. Des.*, 2013, **1**, 2732–2742.

41 O. Allahdin, E. Foto, N. Poumayé, O. Biteman, J. Mabingui and M. Wartel, Modeling of Fixed Bed Adsorption Column Parameters of Iron(II) Removal Using Ferrihydrite Coated Brick, *Am. J. Anal. Chem.*, 2023, **14**, 184–201.

42 A. Reffras, *Etude de l'adsorption de colorants organiques (rouge nylosan et bleu de méthylene) sur des charbons actifs préparés à partir du marc de café*, Université Mentouri Constantine, 2017, 1.

43 G. Bohart and E. Adams, Some aspects of the behavior of Charcoal with respect to Chlorine, *J. Am. Chem. Soc.*, 1920, **42**(3), 523–544.

44 Y. H. E. E. Yoon and J. H. Nelson, Application of Gas Adsorption Kinetics I. A Theoretical Model for Respirator Cartridge Service Life, *Am. Ind. Hyg. Assoc., Q.*, 2010, 8894.

45 M. L. Dlamini, M. Bhaumik, K. Pillay and A. Maity, Polyaniline nanofibers, a nanostructured conducting polymer for

the remediation of Methyl orange dye from aqueous solutions in fixed-bed column studies, *Heliyon*, 2021, **7**(10), e08180, DOI: **10.1016/j.heliyon.2021.e08180**.

46 J. Mohanta, B. Dey and S. Dey, Highly porous iron-zirconium binary oxide for efficient removal of congo red from water, *Desalin. Water Treat.*, 2020, **189**, 227–242, DOI: **10.5004/dwt.2020.25570**.

47 M. S. F. Al, H. Amel, L. Hecini, A. I. Osman and G. Gamal, Valorizing date palm spikelets into activated carbon – derived composite for methyl orange adsorption: advancing circular bioeconomy in wastewater treatment—a comprehensive study on its equilibrium, kinetics, thermodynamics, and mechanisms, *Environ. Sci. Pollut. Res.*, 2024, **31**(38), 50493–50512.

48 P. Zheng, B. Bai, W. Guan, H. Wang and Y. Suo, Fixed-bed column studies for the removal of anionic dye from aqueous solution using TiO_2@glucose carbon composites and bed regeneration study, *J. Mater. Sci.: Mater. Electron.*, 2016, **27**(1), 867–877.

49 L. Zhao, W. Zou, L. Zou, X. He, J. Song and R. Han, Adsorption of methylene blue and methyl orange from aqueous solution by iron oxide-coated zeolite in fi xed bed column: predicted curves, *Desalin. Water Treat.*, 2010, **22**(1–3), 258–264.

50 S. Majumdar, A. Baishya and D. Mahanta, Kinetic and Equilibrium Modeling of Anionic Dye Adsorption on Polyaniline Emeraldine Salt: Batch and Fixed Bed Column Studies, *Fibers Polym.*, 2019, **20**(6), 1226–1235.

51 D. M. Guo, Q. D. An, R. Li, Z. Y. Xiao and S. R. Zhai, Ultrahigh selective and efficient removal of anionic dyes by recyclable polyethylenimine-modified cellulose aerogels in batch and fixed-bed systems, *Colloids Surf., A*, 2018, **555**, 150–160, DOI: **10.1016/j.colsurfa.2018.06.081**.